Lab on a Chip

Accepted Manuscript

ROYAL SOCIETY OF CHEMISTRY

www.rsc.org/loc

Journal Name

COMMUNICATION

Microwave Temperature Measurement in Microfluidic Devices

David Y. Wong,[a] Gurkan Yesiloz,[a] Muhammed S. Boybay[a,b] and Carolyn L. Ren[a*]

Received 00th January 20xx,
Accepted 00th January 20xx

DOI: 10.1039/x0xx00000x

www.rsc.org/

In spite of various existing thermometry methods for microfluidic applications, it remains challenging to measure temperature of individual droplets in segmented flow since fast moving droplets do not allow sufficient exposure time demanded by both fluorescence based techniques and resistance temperature detector. In this contribution, we present a microwave thermometry method that is non-intrusive and requires minimal external equipment. This technique relies on the correlation of fluid temperature with the resonance frequency of a microwave sensor that operates at a GHz frequency range. It is a remote yet direct sensing technique, eliminating the need for mixing fluorescent dyes with the working fluid. We demonstrated that the sensor operates reliably over multiple tests, and is capable of both heating and sensing. It measures temperature to within ±1.2℃ accuracy, and can detect temperature of individual droplets.

Temperature measurement and control is critical in chemical processes. For example, amplification performance of polymerase chain reactions is significantly affected by temperature deviations as small as 2°C[1]. In the Reamer-Tiemann reaction, thermal runaway and boiling are issues that must be avoid through quick feedback control, which is only possible if instantaneous temperature measurement is available[2]. In other occasions such as quantum dot synthesis, temperature must be controlled during crystallization in order to attain desired photoluminescence peak and full width at half-maximum[3], which would also require accurate temperature measurement for controlling purposes.

There have been many techniques reported for measuring temperature profiles in microfluidic chips [4-8]. However, precise temperature measurement at micro-scale is still a difficult task because of the rapid thermal diffusion and short dissipation timescales, or due to complications in micro-fabrication. Of these, a common technique is the resistance temperature detector (RTD), which is a simple solution that requires minimal external equipment. RTDs are relatively easier to fabricate and suitable for steady state temperature monitoring [9]. Response time of RTD is slow due to the heat transfer between the sample fluid and sensor. Moreover, segmented droplets are often smaller than the sensor footprint required for RTD operation, resulting in significant error.

To measure temperature of microfluidic sample in-situ, methods based on fluorescence intensity ratio (FIR) are often used. The quantum yield of some fluorescence dyes such as Rhodamine B is temperature dependent, which allows spatial temperature distribution to be measured with less than 3.5℃ uncertainty[10-11]. To improve accuracy, fluorescent systems with ultralow temperature coefficient are required[4]. In addition, this method works well with glass-based materials, but is not compatible with porous chip materials such as poly(dimethylsiloxane) (PDMS) because dye particles tend to diffuse into and adsorb to channel walls, creating artificial fluorescent intensities. Driven by the popular use of PDMS for microfluidic chip fabrication and the high spatial resolution of temperature measurements enabled by Rhodamine B, several techniques have been developed to overcome such challenges [12-13]. Other molecular probes such as Fluorescein has no direct temperature dependence in its fluorescent intensity, but has a temperature dependent pH change which could be used to measure temperature if a pH-temperature sensitive buffer is available for use. As a general temperature probe, (CdSe)ZnS quantum dot is superior since its emission and absorption spectra can be tuned during growth, but synthesis and fabrication into usable form such as coated beads remain costly[14]. The major source of error for all FIR based methods is the non-uniform local probe concentration, and fluctuation in excitation intensity. By employing two different dyes with separate emission spectra and two simultaneously operating cameras, temperature can be related to the ratio between the two emission spectra, unaffected by concentration and source fluctuation[15-16]. If picosecond photo counting equipment is available, fluorescence life time (FL) can be used to measure temperature instead. This method is not affected by

[a] Department of Mechanical and Mechatronics Engineering, University of Waterloo, 200 University Avenue West, Waterloo, Ontario, N2L 3G1, Canada.
[b] Department of Computer Engineering, Antalya International University, Universite Caddesi No:2, 07190 Antalya, Turkey

† Footnotes relating to the title and/or authors should appear here.
Electronic Supplementary Information (ESI) available: [details of any supplementary information available should be included here]. See DOI: 10.1039/x0xx00000x

concentration and excitation source, and can attain 3D temperature distribution of ±1℃ accuracy[17-18].

Predating the FIR and FL methods, cholesteric liquid crystals (TLC) are used to measure temperature at ±0.1℃ accuracy at the expense of a narrow operating range[1-2, 19]. Its high accuracy results from drastic hue change within a range of 1~2℃. Despite its high accuracy, the high viscosity and large bead size after necessary encapsulation have limited the use of TLC in microfluidic devices. Other sensing methods exist, such as through observing Brownian motion of particles under micro PIV. Temperature can be correlated to ±3℃ accuracy with this method[20]. Raman spectroscopy can detect temperature based on stretching modes of hydrogen bond, but suffers from a long acquisition time up to 16.5s due to Raman scattering's inherent weak intensity[21]. Temperature can also be measured based on acoustic time of flight[22]; from changes in refractive index using interferometry[23]; as well as using nuclear magnetic resonance spectroscopy [24].

A recent development in microfluidics heating involves the use of microwave [25-26]. Herein, we present a microwave-based method that can measure individual droplet temperature with accuracy comparable to FIR methods without the need of sample preparation, and requires only a single commercially available device. Previously, we have shown that this device is also capable of selectively heating individual droplets and content sensing in microfluidic chips [27-28].

Experimental

The microwave sensor is composed of two planar concentric ring-shaped electrodes. The outer ring connects to a microwave source via a coaxial cable; the inner ring is electromagnetically coupled to the outer ring. The inner ring has a capacitive discontinuity that lies over the fluid channel. By detecting the change in the fluid permittivity, its temperature can be measured[29]. This permittivity change is represented by the sensor's change in its resonance frequency. Based on the transmission line theory, the sensor can be treated as a load with complex impedance and temperature can be correlated to the reflective coefficient or single port scattering parameter (S_{11}) of the sensor, which is defined as the ratio between the incident and reflected voltage.

A spectral measurement of the scattering parameter allows the extraction of the resonance frequency and quality factor, which in this case indicates the selectivity at which microwave is being absorbed by the working fluid. The resonance frequency, quality factor, and absorption magnitude are used to establish a relationship with temperature. The sensor is tested multiple times to demonstrate repeatability, and then used to measure droplet temperature.

The microwave sensor is fabricated from copper coated glass slides (EMF Corporation). The glass slide is first patterned with S1813 positive photoresist (Rohm-Haas), then electroplated ($0.2M\ CuSO_4$, $0.1M\ H_3BO_3$ and $0.1M\ H_2SO_4$) and etched with ferric chloride to achieve a thickness of around 5µm. It is than covered with a thin layer of Sylgard 184 PDMS (Dow Corning) to isolate electrodes from the working fluid. In order to prevent evaporation at high temperature, experiments are run at relatively high pressures which still result in deformation in PDMS channels and inconsistent measurements. The problem was overcome by adding a hard PDMS layer that contains all the channels. The sandwiched PDMS chip is fabricated using standard soft lithography protocol[30]. The channel design consists of a T-junction droplet generator and serpentines to achieve a residence time beyond 80s, such that during calibration, the working fluid is heated to steady state temperature before reaching the microwave sensor. The chip is assembled using plasma bonding followed by Aquapel surface treatment (PPG Industries) in order to obtain a hydrophobic surface. A SMA connector (Cinch Connectivity Solutions Johnson) is soldered on as the last step.

The experimental setup, shown in Figure 1, consists of a fan for enhanced cooling, and a hotplate (PH-121S, MSA Factory) for measuring and controlling the surface temperature. The hotplate is recently calibrated and rated for ±0.05℃ accuracy, and is mounted in an inverted position to allow microscope observation. The chip is pressed on to the hotplate by spring clips, separated by glass slides with a total thickness of 4.3mm. The glass slides are necessary for electrical insulation. Thermopaste (OT-201, Omega) is applied on all contact surfaces to reduce thermal resistance. Throughout the experiments, Fluorinert FC-40 with 2% custom-made surfactant (chemical structure of PFPE-PEG-PFPE) is used as the continuous phase and ultra-pure water as the dispersed phase. The microscope is used merely for observation, and is not involved with measurement. For microwave measurement, a vector network analyzer (VNA) (MS2028C, Anritsu) is used. The VNA has a frequency resolution of 0.05 MHz and a magnitude resolution of 0.07dB.

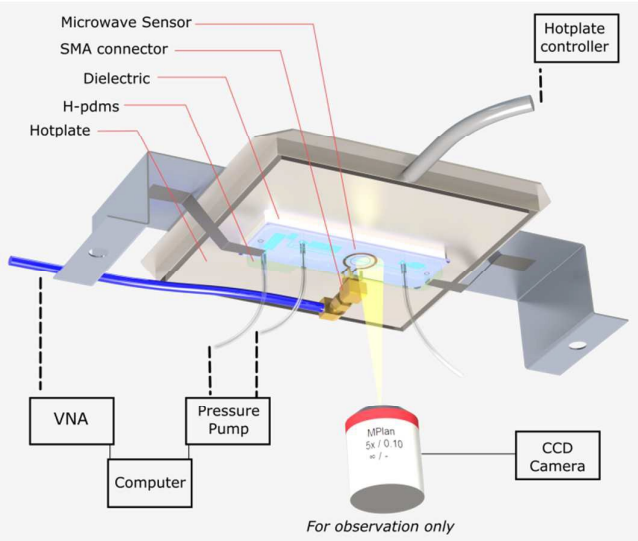

Figure1. Experiment setup schematic. The microfluidic chip with embedded microwave sensor is attached to the hotplate. The whole unit is mounted onto the microscope for visualization purposes.

Journal Name

COMMUNICATION

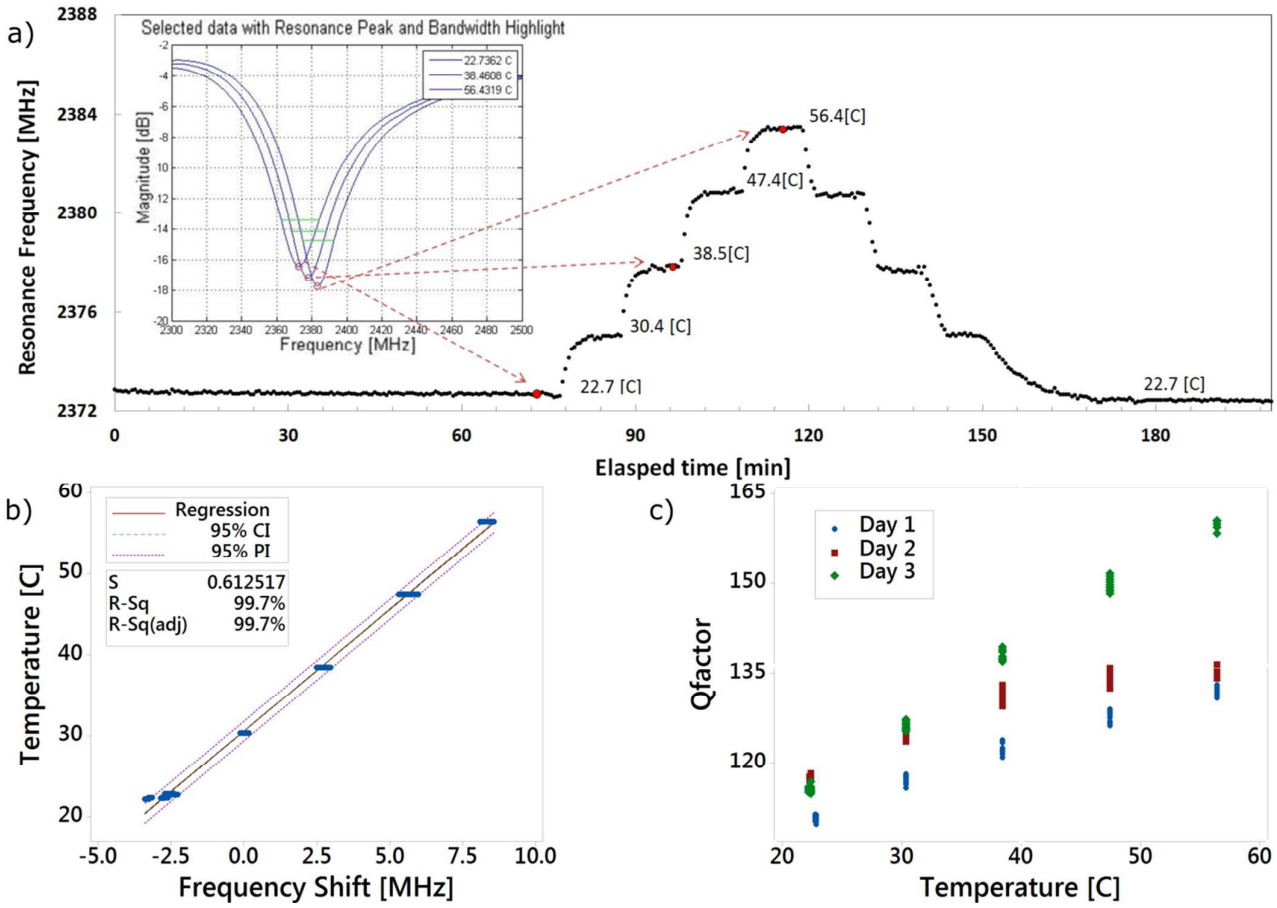

Figure2. a) Resonance frequency vs. time, as temperature is increased and then decreased. Subplot shows raw data (spectral measurement) at three temperature set points. The resonance peak is marked with red circle, while the half-power bandwidth is labelled green. b) Temperature vs. resonance frequency shift calibration, all data from three separate tests are plotted, and 95% confidence and prediction intervals are shown. c) Quality factor vs. temperature, relationship varies from test to test, suggesting that quality factor is easily affected by setup change.

Results and Discussion

Single phase temperature measurement

At first, the sensor is tested on single phase water. The continuous flow provides enough time to sweep through a large frequency range, allowing the resonance frequency and quality factor to be identified. Figure 2a demonstrates the resonance frequency response of our microwave sensor to the different temperature increments. It can be seen that higher temperature values cause increase in the resonance frequency. The inset shows the behaviour of the frequency sweep and reflection (S_{11}) corresponding to temperatures of 22.7 ℃, 38.5 ℃ and 56.4 ℃, respectively. Over the course of three hours, the surface temperature of the hotplate is increased in steps from room temperature to 60℃, and then decreased back to room temperature before new experiments are conducted. A fan is turned on when necessary to enhance cooling. For each temperature set point, frequency sweep data is collected at 0.5min intervals, each containing 4000 data points in S_{11} measurements. The resonance frequency for each set of measurements is identified by locating where the maximum absorption happens. The quality factor is calculated using Equation (1), where BW is the half-power fractional bandwidth, Q is the quality factor and f denotes the resonance frequency of the microwave sensor. To exclude the thermal transient effects of the hotplate, only data set attained in the last 5 minutes at each temperature step are used for further processing.

$$Q = \frac{f_{resonance}}{BW_{half-power}} \quad (1)$$

Since the channel is separated from the hotplate surface by glass slides, a correction is added to correlate the fluid temperature to hotplate surface temperature. The correction function is obtained by inserting a thermo-couple into the channel of a dummy chip with PDMS thickness equals to the actual chip used [See ESI S1]. The dummy chip is mounted in the inverted hotplate setup; the temperature difference is measured repeatedly and used to create the correction function. Deviation in ambient temperature from the testing condition will result in error in the correction function; therefore, a 1-dimensional heat transfer model was created to evaluate effects of changing room temperature on the glass slide correction [See ESI S2]. The model predicts temperature differences matching those from the measurements, and shows that room temperature fluctuation contributes to less than 0.1℃ error in the correction function. In lieu of this correction method, an attempt was made to measure channel temperature directly using a RTD sensor, but fabrication of both microwave and RTD sensor on the same chip was difficult. Fluorescence thermometry was also performed using fluorescein with Tris-HCL buffer. Results were later rejected since typical FIR based methods induce larger errors than that of the hotplate correction method. [See ESI S3]

The aforementioned single phase frequency sweep test was repeated in the following two days to evaluate the sensor's repeatability [See ESI S4], and a curve fit was performed using linear regression including all three sets of data. While Figure 2b shows a linear relationship between the resonance frequency and temperature that is unchanged from test to test, Figure 3b shows that the quality factor trend varies day by day between tests. The relationship between resonance frequency and temperature is provided in Table 1. It is observed that setup differences such as cable routing have significant influence on the resonance peak shape, and such influence is quantified by the half-power bandwidth, eventually affecting the quality factor. The contrasting behaviour between the quality factor and frequency shift suggests that the latter is a good temperature indicator uncompromised by external set up changes. Based on the curve fit data, the temperature sensitivity on the resonance frequency is 0.33 MHz/℃. Given that the VNA is accurate up to 0.05MHz, the temperature measurement resolution is 0.15℃. Prediction intervals are used to estimate that temperature measurement will have an accuracy of ±1.2℃.

Droplet temperature measurement

Compared with single phase flow, fast moving droplets reduce the available time interval when the sample passes through the microwave sensor. If applied directly, the spectral approach described above will impose a speed limit that strike a trade-off between droplet speed and temperature resolution. Consequently, a single frequency temperature measurement method is proposed below.

For the droplet temperature measurement, we utilized the change of reflection coefficient at a fixed frequency to calibrate its temperature dependence. This method relies on the large difference in dielectric constant between water (80.1 @ 25 ℃) and oil (2.7 for silicone oil, 1.9 for FC-40, 2.0 for hexadecane); such that practically all microwave energy is absorbed by the aqueous droplets instead of by the continuous oil phase. While changing droplet material or composition will require a separate temperature calibration, the effects of different oil composition or varying oil temperature is negligible. Figure 3a shows an excerpt of single frequency data at 2317MHz, the crests correspond to continuous oil phase, and the troughs correspond to water droplets at two different temperatures. During experiments, cable routing is fixed in space to eliminate error induced by setup changes, and hotplate temperature is varied between room temperature and 70℃. Notice that water-to-oil volume ratio increases with temperature, which is caused by viscosity temperature dependence, resulting in a changing capillary number which affects droplet generation. As explained below, the increase of droplet length has no effect on temperature measurement.

A cut off magnitude is used to discard the measurements from continuous oil phase and isolate the data for each droplet. For each droplet, the minimum magnitude is calculated and used as a temperature indicator. The calibration is different at other frequencies, and the temperature dependence increases when moving closer towards the resonance peak, as shown in Figure 3b. In this test, 2317MHz is chosen to be reasonably close to the resonance peak, resulting in a sensitivity of 0.27 dB/℃**,** which corresponds to a 0.26 ℃ resolution based on the VNA's ability in resolving S_{11}magnitude. Figure 3c shows the curve fit over 163 data points; residuals from the linear regression suggests that a 3rd degree polynomial provides a good description of the relationship between absorption magnitude and temperature.

Droplet temperature measurement using this method has an accuracy of ±1.17℃. The relationship between S_{11} magnitude at 2317MHz and temperature is listed in Table 1. Varying the size of droplet will have no effects on temperature measurement, as long as droplet length, l, is larger than the microwave sensor diameter l_0 ($200\mu m$). The maximum allowed droplet velocity, v_{max}, for registering measurement depends on the sampling period T_s of the microwave circuitry, and can be calculated from equation (2). In our previous work[28], a custom microwave circuit with $T_s = 10\mu m$ was employed, and has shown to achieve consistent measurement for droplets being generated at 2 kHz.

$$v_{max} = \frac{l - l_0}{2T_s} \quad (2)$$

During experiments, it was observed that single phase water upstream of droplet generation would evaporate, while water droplets downstream would remain in liquid phase at even higher temperature. This suggests a higher local pressure within droplet contributed by the interfacial surface tension, as described in Equation (3). Since the microwave sensor is a

local heating and sensing device, the Laplace pressure could be exploited to achieve stable operation at elevated temperature.

$$P_{droplet} - P_{continuous} = \frac{2 \cdot \gamma}{R_{interface}} \quad (3)$$

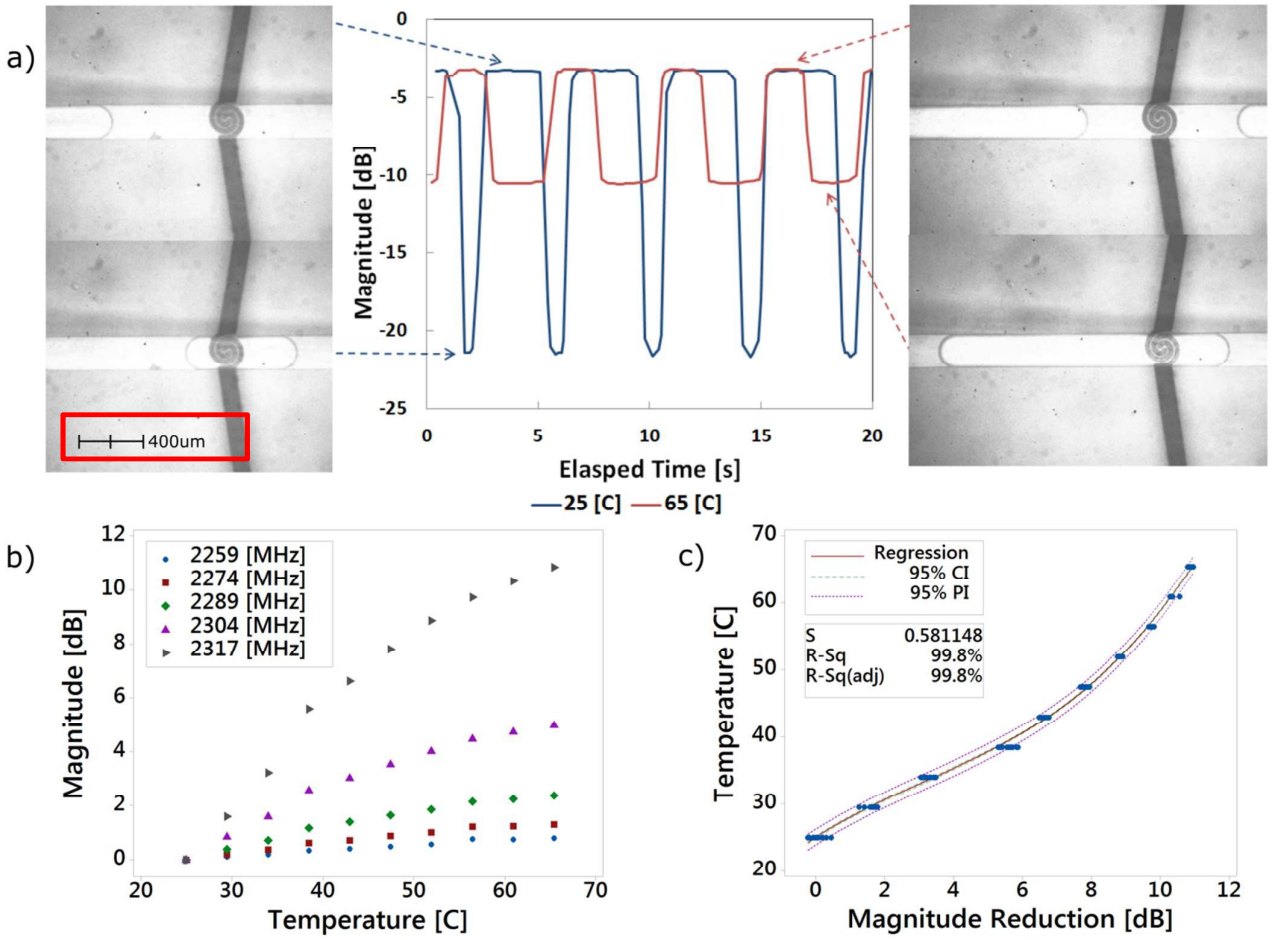

Figure3. a) Single frequency S11 measurement magnitude vs. time. Pictures on the left show droplet crossing sensor under room temperature, and corresponds to the blue trace. Pictures on the right shows droplet crossing sensor at elevated temperature, and corresponds to the red trace. b) S11 magnitude vs. temperature at various frequencies, sensitivity increases as test frequency moves towards resonance frequency. c) Temperature vs. S11 magnitude reduction calibrated at 2317MHZ. 3rd order polynomial is used for calibration fit, with 95% confidence and prediction intervals shown.

Table1. Summary of the microwave temperature measurement method

Methods	Frequency Shift (for Single Phase)	Magnitude reduction (for Droplet)
Hardware Resolution	0.15 [°C]	0.26 [°C]
Sensitivity	0.33 [MHz/°C]	0.27 [dB/°C]
Reference Temperature	30.4 [°C]	25.0 [°C]
Calibration	$T = 2.999(F - F_0) + 30.59$	$T = 0.03076(M - M_0)^3 - 0.2966(M - M_0)^2 + 3.259(M - M_0) + 25.04$
Fit Residuals	0.997	0.998
95% Prediction Interval	±1.20 [°C]	±1.17 [°C]
Source of Error	Ambient Temperature Variation	Sensor Drift over Long Period
Effects	0.099 [°C/°C] @ 50°C	0.084 [MHz/hr]@ 50°C 0.25 [°C/hr] @ 50°C

Conclusions

In conclusion, the microwave sensor is a viable temperature measuring device. It has comparable or better accuracy than common fluorescence-based methods, but does not require the use of intrusive fluorescent dyes, and can measure individual droplet temperature without exposure time limitations imposed by optical equipment. Relationships and performance of frequency shift calibration and magnitude reduction calibration is summarized in Table 1. It should be noted that the listed accuracies and resolution values are preliminary in nature, and contain many areas for improvement. For example, the microwave sensor on the single phase chip is observed to exhibit a slight drift over time at elevated temperature, which is quantified at 0.25°C/hr [See ESI S5]. Such a drift is accounted for in the calibration process and have no effect on the sensor's day to day repeatability, as demonstrated in the three repeating tests. However, it does contribute to error within the 3 hour calibration period. The drift is likely resulted from continuous absorption of water into PDMS, and could be eliminated by changing substrate material. As for the droplet calibration method, further

explorations in the sensor design can make it less susceptible to setup changes, and potentially much higher accuracy.

Also, the slow droplet generation speed shown in Figure 3a is a limitation imposed by the VNA. Even though the VNA has a KHz sampling rate when performing frequency sweeps, it can only output to computer at 6Hz when obtaining single frequency measurements through the NI-VISA protocol. With equipment intended for single frequency instead of spectral measurement, the single frequency calibration method can operates at much higher speed.

Lastly, the tested temperature range is by no means the operation limit of the sensor. Experiments are limited to temperatures above which evaporation occurs. Attempt to suppress evaporation by applying higher pressure often lead to irreversible damage to the bonding between glass and PDMS. With a stronger chip, the microwave sensor will remain sensitive at much higher temperature.

References

1 Chaudhari, A. M., Woudenberg, T. M., Albin, M., & Goodson, K. E., *Microelectromechanical Systems, Journal of*, 1998, *7*(4), 345-355.
2 Iles, A., Fortt, R., & de Mello, A. J., *Lab on a Chip*, 2005, *5*(5), 540-544.
3 Chan, E. M., Alivisatos, A. P., & Mathies, R. A., *Journal of the American Chemical Society*, 2005, *127*(40), 13854-13861.
4 Mao D., Liu X., Qiao Q., Yin W., Zhao M., Cole J.M., Cui J. and Xu Z., Analyst, 2005, 140, 1008-1013.
5 Chen Y.Y. and Wood A. W., *Bioelectromagnetics*, 2009, 30, 583-590.
6 Gui L. and Ren C.L., *Applied Physics Letters*, 2008, 92(2), 024102.
7 Schreiter K.M., Glawdel T., Forrest J.A. and Ren C.L., *RSC Advances*, 2013, 3(38), 17236-17243.
8 Bennet M.A., Richardson P.R., Arlt J., McCarthy A., Buller G.S. and Jones A.C., Lab Chip, 2011, 11(22), 3821-3828.
9 Dames, Chris. *Encyclopedia of Microfluidics and Nanofluidics. Springer US*, 2008, 1782-1790.
10 Ross, D., Gaitan, M., & Locascio, L. E., *Analytical chemistry*, 2001, *73*(17), 4117-4123.
11 Gosse, Charlie, Christian Bergaud, and Peter Löw., *Thermal Nanosystems and Nanomaterials. Springer Berlin Heidelberg*, 2009, 301-341.
12 Samy, R., Glawdel, T., & Ren, C. L., *Analytical chemistry*, 2008, *80*(2), 369-375.
13 Glawdel, T., Almutairi, Z., Wang, S., & Ren, C. L., *Lab on a Chip*, 2009, *9*(1), 171-174.
14 Walker, G. W., Sundar, V. C., Rudzinski, C. M., Wun, A. W., Bawendi, M. G., & Nocera, D. G., *Applied Physics Letters*, 2003, *83*(17), 3555-3557.
15 Sakakibara, J., & Adrian, R. J., "Whole field measurement of temperature in water using two-color laser induced fluorescence." *Experiments in Fluids*, 1999, *26*(1-2)
16 Natrajan, V. K., & Christensen, K. T., *Measurement Science and Technology*, 2008, *20*(1), 015401.
17 Okabe, K., Inada, N., Gota, C., Harada, Y., Funatsu, T., & Uchiyama, S., *Nature communications, 2012*, *3*, 705.
18 Benninger, R. K., Koç, Y., Hofmann, O., Requejo-Isidro, J., Neil, M. A., French, P. M., & deMello, A. J., *Analytical chemistry*, 2006, *78*(7), 2272-2278.
19 Dabiri, D., & Gharib, M., "Digital particle image thermometry: the method and implementation." *Experiments in Fluids*, 1991, *11*(2-3)
20 Hohreiter, V., Wereley, S. T., Olsen, M. G., & Chung, J. N., *Measurement science and technology*, 2002, *13*(7), 1072.
21 Kuriyama, R., & Sato, Y., *Measurement Science and Technology*, 2014, *25*(9), 095203.
22 Yaralioglu, G., *Sensors and Actuators A: Physical*, 2011, *170*(1), 1-7.
23 Easley, C. J., Legendre, L. A., Roper, M. G., Wavering, T. A., Ferrance, J. P., & Landers, J. P., *Analytical chemistry*, 2005, *77*(4), 1038-1045.
24 Lacey, M. E., Webb, A. G., & Sweedler, J. V., *Analytical chemistry*, 2000, *72*(20), 4991-4998.
25 Issadore, D., Humphry, K. J., Brown, K. A., Sandberg, L., Weitz, D. A., & Westervelt, R. M., *Lab on a Chip*, 2009, *9*(12), 1701-1706.
26 Abduljabar, Ali Amin, et al., *Microwave Theory and Techniques, IEEE Transactions on*, 2015, 63(11), 3681-3690.
27 Boybay, M. S., Jiao, A., Glawdel, T., & Ren, C. L., *Lab on a Chip*, 2013, *13*(19), 3840-3846.
28 Yesiloz G., Boybay M.S. and Ren, C. L., *Lab on a Chip*, 2015, *15*, 4008-4019.
29 Meissner, Thomas, and Frank J. Wentz. *Geoscience and Remote Sensing, IEEE Transactions on,* 2004, 42(9), 1836-1849.
30 Qin, D., Xia, Y., & Whitesides, G. M., *Nature protocols*, 2010, *5*(3), 491-502.